

SCIENTIFIC REPORTS



OPEN

Understanding the Control of Singlet-Triplet Splitting for Organic Exciton Manipulating: A Combined Theoretical and Experimental Approach

Received: 23 January 2015

Accepted: 07 May 2015

Published: 10 July 2015

Ting Chen¹, Lei Zheng¹, Jie Yuan¹, Zhongfu An^{1,2}, Runfeng Chen¹, Ye Tao¹, Huanhuan Li¹, Xiaoji Xie² & Wei Huang^{1,2}

Developing organic optoelectronic materials with desired photophysical properties has always been at the forefront of organic electronics. The variation of singlet-triplet splitting (ΔE_{ST}) can provide useful means in modulating organic excitons for diversified photophysical phenomena, but controlling ΔE_{ST} in a desired manner within a large tuning scope remains a daunting challenge. Here, we demonstrate a convenient and quantitative approach to relate ΔE_{ST} to the frontier orbital overlap and separation distance *via* a set of newly developed parameters using natural transition orbital analysis to consider whole pictures of electron transitions for both the lowest singlet (S_1) and triplet (T_1) excited states. These critical parameters revealed that both separated S_1 and T_1 states leads to ultralow ΔE_{ST} ; separated S_1 and overlapped T_1 states results in small ΔE_{ST} ; and both overlapped S_1 and T_1 states induces large ΔE_{ST} . Importantly, we realized a widely-tuned ΔE_{ST} in a range from ultralow (0.0003 eV) to extra-large (1.47 eV) *via* a subtle symmetric control of triazine molecules, based on time-dependent density functional theory calculations combined with experimental explorations. These findings provide keen insights into ΔE_{ST} control for feasible excited state tuning, offering valuable guidelines for the construction of molecules with desired optoelectronic properties.

The ultimate challenge in manipulating conjugated molecules^{1,2} for optoelectronic applications is to develop universal approaches capable of controlling excited states for efficient electron-light conversions, affording not only conventional fluorescence³ and phosphorescence⁴, but also many other photophysical phenomena including triplet-triplet annihilation (TTA)⁵, singlet fission (SF)⁶, and thermally activated delayed fluorescence (TADF)⁷. The rich photophysical properties of organic molecules have led to many revolutionary developments in organic electronics⁸. Notably, the TTA compounds, which can harvest one singlet exciton from two low-lying triplet excitons, can benefit OLEDs with improved external quantum efficiency (EQE) theoretically up to 12.5% by harvesting the 75% electronically generated triplet excitons to produce singlet excitons for fluorescence⁹; the SF process, which transforms a singlet exciton into two triplet excitons on neighboring molecules with EQE up to 200%, is especially attractive for solar cells in providing doubled photocurrent from high-energy photons¹⁰; the recently developed TADF materials by

¹Key Laboratory for Organic Electronics and Information Displays & Institute of Advanced Materials, Jiangsu National Synergistic Innovation Center for Advanced Materials, Nanjing University of Posts & Telecommunications, 9 Wenyuan Road, Nanjing 210023, China. ²Key Laboratory of Flexible Electronics & Institute of Advanced Materials, Jiangsu National Synergistic Innovation Center for Advanced Materials, Nanjing Tech University, 30 South Puzhu Road, Nanjing 211816, China. Correspondence and requests for materials should be addressed to R.C. (email: iamrfchen@njupt.edu.cn) or W.H. (email: wei-huang@njtech.edu.cn)

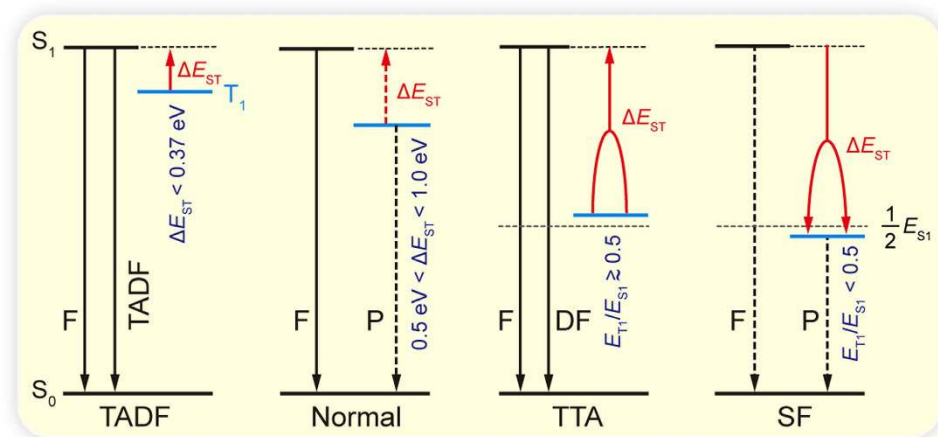


Figure 1. Energy level diagrams depicting diversified photophysical processes determined by singlet-triplet splitting (ΔE_{ST}) between energies of the lowest singlet (E_{S1}) and triplet (E_{T1}) excited states. Noted that F, P, DF, TADF, TTA, SF represent fluorescence, phosphorescence, delayed fluorescence, thermally activated delayed fluorescence, triplet-triplet annihilation, and singlet fission, respectively. The weak emissions and transitions are in dotted line.

harvesting 100% triplet excitons *via* reversed intersystem crossing have achieved EQEs of 20.6% in blue and 30.0% in green TADF OLED devices^{11,12}, which are comparable to the heavy metal-based phosphorescent emitters^{13,14}.

To control the triplet/singlet excited states in a designed manner for a desired optoelectronic property, the rational adjustment of the singlet-triplet energy gap (ΔE_{ST}) between the first singlet (S_1) and triplet (T_1) excited states is the key. Typically in Fig. 1, when ΔE_{ST} normally laid between 0.5 and 1.0 eV⁷ in conventional compounds is reduced ($\Delta E_{ST} \leq 0.37$ eV)¹⁵, TADF could be resulted *via* activated endothermic RISC process from T_1 to S_1 by the thermal motions of the molecule atoms for the *E*-type delayed fluorescence¹⁶. Meanwhile, when the ΔE_{ST} is increased and the energy of two triplet excitons are close to, or larger than, one singlet exciton ($E_{T1}/E_{S1} \geq 0.5$), TTA could happen between triplet exciton interaction pair following the spin statistics rule¹⁷. SF process, either isoergic or slightly exoergic in producing two triplet excitons with a net spin of zero, is spin-allowed and favorable for fast generation of doubled triplet excitons from high-lying singlet excitons, when S_1 excitation energy is comparable with twice the energy of T_1 excitation ($E_{T1}/E_{S1} < 0.5$)¹⁸.

Extensive efforts have been so far devoted to reducing ΔE_{ST} via separated the highest occupied molecular orbital (HOMO) and the lowest unoccupied molecular orbital (LUMO) strategy to construct efficient TADF molecules⁸. In contrast, TTA and SF molecules were designed by enhancing HOMO-LUMO overlap to the maximum possible degree with enlarged ΔE_{ST} ^{18,19}. Consequently, efficient TADF compounds were generally found in donor-acceptor (D-A) molecules²⁰, while TTA and SF compounds were mostly observed in alternant hydrocarbons with an even number of carbons in conjugated close-shell S_0 systems¹⁸. Considering the four-electron picture transformation of SF process, the involvement of charge transfer (CT) character through either inter- or intra-molecular D-A interactions is also crucial for the ultrafast fission^{21,22}. However, despite these advances to date, it remains a challenge to rationally manipulate ΔE_{ST} in a large scale *via* subtle molecular structure adjustments to produce energy levels applicable not only for TADF but also for TTA and SF processes.

The lack of quantitative means in describing HOMO-LUMO overlap and separation extents should be a main obstacle in establishing accurate relations between ΔE_{ST} and molecular structures. Here, we demonstrate a convenient approach in quantifying the frontier orbital overlap and separation with a set of new parameters in both S_1 and T_1 states. With the aid of these quantitative parameters, we proposed a molecular symmetry controlling strategy to fine tune the excited state energy levels for accommodation of excitons with diversified spin states and for the support of their varied excited state transfer processes following corresponding photophysical mechanisms of TADF, TTA, and SF. In a typical example demonstrated in 1,3,5-triazine-based molecules, we designed a series of symmetric and asymmetric triazines and successfully realized a widely varied ΔE_{ST} in a range from ultralow (0.0003 eV) for TADF and extra-large (1.47 eV) for SF according to time-dependent density functional theory (TD-DFT) calculations and experimental measurements of selectively synthesized molecules. The widely-tuned ΔE_{ST} *via* a subtle symmetric control in a uniform molecular architecture is attractive not only for providing a practical guide for material design of TADF, TTA and SF processes, but also for developing a better understanding of the factors that influence the energy levels and spin states of the excited states of organic optoelectronic molecules.

Results

Theoretical considerations. The lowest singlet-triplet splitting (ΔE_{ST}) between the molecular energies at the lowest singlet (E_{S1}) and triplet (E_{T1}) excited states were equal to twice of the electron exchange energy (J) as illustrated in equation (1) and (2), where J is determined by the spatial separation and overlap extents of HOMO (φ_H) and LUMO (φ_L)²³. From equation (3), the ΔE_{ST} is closely related to the frontier orbital overlap extent and separation distance at S_0 state; higher overlap of HOMO and LUMO and smaller spatial separation ($r_1 - r_2$) lead to higher J and ΔE_{ST} .

$$\Delta E_{ST} = E_{S1} - E_{T1} = 2J \quad (1)$$

$$J = \iint \varphi_L(1) \varphi_H(1) \left(\frac{e^2}{r_1 - r_2} \right) \varphi_L(2) \varphi_H(2) dr_1 dr_2 \quad (2)$$

$$\Delta E_{ST} = \iint \varphi_L(1) \varphi_H(1) \left(\frac{2e^2}{r_1 - r_2} \right) \varphi_L(2) \varphi_H(2) dr_1 dr_2 \quad (3)$$

$$I_{H/L} = \int |\varphi_H(r) \varphi_L(r)| dr \quad (4)$$

$$r_{\text{tot}} = \frac{\sum_k^{\text{all}} r_k f(r_k)}{\sum_k^{\text{all}} f(r_k)} \quad (5)$$

$$r_H = \frac{\sum_k^{\text{all}} r_k f_H(r_k)}{\sum_k^{\text{all}} f_H(r_k)} \quad (6)$$

$$r_L = \frac{\sum_k^{\text{all}} r_k f_L(r_k)}{\sum_k^{\text{all}} f_L(r_k)} \quad (7)$$

$$\langle r_{H/L} \rangle = |r_H - r_L| \quad (8)$$

The orbital overlap extent ($I_{H/L}$) between HOMO (H) and LUMO (L) can be calculated using the overlap integral function of Multiwfn (eq. (4))²⁴. Mean separation distance ($\langle r_{H/L} \rangle$) of HOMO and LUMO can be obtained from the barycenter (r_{tot}) of the absolute value of the corresponding molecular orbitals (equation (5–8))²⁵. Similarly, the overlap extent and mean separation distance between the highest occupied natural transition orbitals (HONTOs) and the lowest unoccupied natural transition orbitals (LUNTOs) at both S_1 (I_S and $\langle r_S \rangle$) and T_1 (I_T and $\langle r_T \rangle$) states were also calculated to give a full-picture analysis of the factors that influence ΔE_{ST} . The detailed definitions and calculations of ΔE_{ST} , $I_{H/L}$, I_S , I_T , $\langle r_{H/L} \rangle$, $\langle r_S \rangle$ and $\langle r_T \rangle$ were presented in Supplementary Information.

Molecular design. Triazine, which possesses high electron affinity and good thermal stability, is chosen as a basic building block to demonstrate our ΔE_{ST} tuning strategy for achieving varied photophysical behaviors of TADF, TTA, and SF in a uniform molecular architecture with symmetry control. The symmetric or asymmetric substitution of various donors or acceptors on three reactive sites of 1,3,5-triazine have resulted in a large number of triazine-based molecules with varied optoelectronic properties²⁶. The competition and coordination effects between the substituents, triazine core, and the D-A molecular architecture significantly tuned the molecular energy structures for the singlet and triplet excitons transitions when excited either optically or electronically, and thus leading to rich and/or exceptional optoelectronic properties²⁷. Here, we designed a series of triazine-based molecules bearing various donors and acceptors substituted asymmetrically (labeled as **A1**, etc.) and symmetrically (labeled as **S7**, etc.) at three substitution sites of the triazine core (Fig. 2, S1 and S2). Triazines of **A2**, **A3**, and **A4**, were experimentally investigated in the literature^{27,28}, while **S9** and **A15** were synthesized in this study (Scheme S1) and their properties were measured to verify the computational results.

Singlet-triplet splitting (ΔE_{ST}). As a key parameter in determining the exciton migration and population on excited states, ΔE_{ST} is of the most importance⁸. To choose an optimal calculation approach to evaluate ΔE_{ST} , TD-DFT methods including B3LYP, PBE0, BMK, M062X, M06HF, and long-range correction functionals (ω B97XD and CAM-B3LYP) at 6–31G(d) basis set level were tested. Compared to the experimental ΔE_{ST} values (Fig. S3 and Table 1), it is clear that B3LYP gives the best prediction of ΔE_{ST} not only for molecules with small ΔE_{ST} but also those with large ΔE_{ST} . In the following investigations,

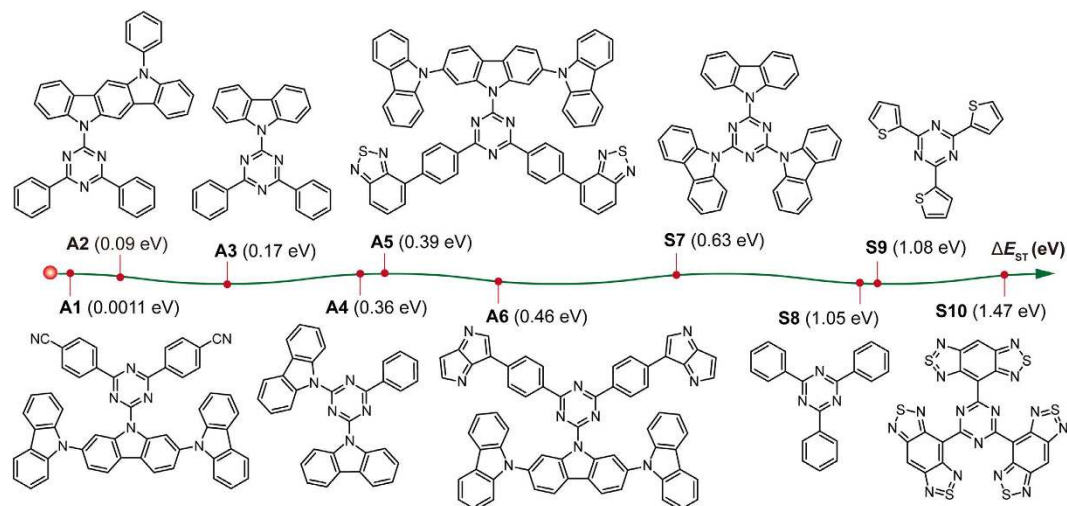


Figure 2. Molecular structures and ΔE_{ST} of asymmetric (A1–A6) and symmetric (S7–S10) triazines.

Compound	A2		A3		A4		S9		A15	
	ΔE_{ST}	$I_{H/L}/I_S/I_T$	ΔE_{ST}	$I_{H/L}/I_S/I_T$	ΔE_{ST}	$I_{H/L}/I_S/I_T$	ΔE_{ST}	$I_{H/L}/I_S/I_T$	ΔE_{ST}	$I_{H/L}/I_S/I_T$
B3LYP	0.09	17/19/25	0.17	24/25/81	0.36	35/42/82	1.08	57/56/80	0.14	23/23/29
PBE0	0.34	17/20/85	0.46	24/26/83	0.64	35/43/83	1.32	56/56/80	0.22	23/24/83
BMK	0.54	17/23/85	0.56	24/30/81	0.67	34/46/83	1.46	56/58/80	0.37	22/26/83
M062X	0.63	17/27/85	0.60	24/34/81	0.59	34/49/83	1.41	55/64/79	0.44	22/29/83
M06HF	0.66	17/72/71	0.84	23/65/81	0.66	34/54/77	1.35	55/69/78	0.90	21/49/83
ω B97XD	1.15	16/70/85	1.23	23/38/84	1.20	34/51/84	1.78	55/69/80	1.08	21/33/84
CAM-B3LYP	1.27	16/69/86	1.27	23/35/85	1.30	34/49/84	1.89	56/69/81	1.07	22/30/84
Exp.	0.02 ²⁶	—	0.34 ²⁵	—	0.45 ²⁵	—	1.01	—	0.19	—

Table 1. Calculated ΔE_{ST} (eV) and frontier orbital overlap extents ($I_{H/L}$, I_S , and I_T (%)) using various functionals at 6–31G(d) basis set level in comparison with experimental data of ΔE_{ST} (eV).

B3LYP/6-31G(d) was selected to predict ΔE_{ST} of the designed compounds that lack experimental explorations. The calculated ΔE_{ST} demonstrate that the asymmetric triazines have small ΔE_{ST} ranging from 0.001 to 0.46 eV, while the symmetric triazines show high ΔE_{ST} up to 1.47 eV. Thus, a wide controlling range of ΔE_{ST} from almost zero to 1.47 eV has been successfully realized in a uniform molecular system by adopting the conventional symmetry control of triazine substituents (Scheme S2).

The origin of the different effects of symmetric and asymmetric substituents on triazines was investigated *via* frontier orbital analysis. Theoretically, the HOMO is dominated by donor moiety while the LUMO is by acceptor moiety²⁹. As a result, the strong donors of tricarbazole and indolocarbazole substituents generally lead to high-lying HOMOs; the strong acceptors of benzonitrile, benzothiazole, and pyrrolo[3,2-b]pyrrole lead to low-lying LUMOs³⁰; the LUMOs and HOMOs of the symmetric triazines are degenerated due to their symmetric molecular structures. The electron density distributions of the triazines also support the above analysis, where the HOMOs are delocalized on the donor moieties and the LUMOs are on the acceptor moieties (Fig. S4 and S5). The asymmetric triazines tend to produce asymmetric distributions of electron density, leading to clearly separated HOMOs and LUMOs. This distinct difference of the frontier orbital distributions between symmetric and asymmetric triazines should be the main reason for their distinct difference in ΔE_{ST} .

HOMO-LUMO overlap extent. To give a quantitative investigation of HOMO-LUMO overlap, their overlap extent ($I_{H/L}$) was calculated using Multiwfn²⁴. As illustrated in Fig. 3a, ΔE_{ST} gradually increases from A1 to S10, when molecular symmetry changes from asymmetric to symmetric with increasing $I_{H/L}$. However, in the cases of compounds A5 and A6, despite their obvious HOMO-LUMO separation with low $I_{H/L}$ and comparable average HOMO-LUMO separation distance ($\langle r_{H/L} \rangle$) to that of A1 which has an ultralow ΔE_{ST} , they exhibit quite large ΔE_{ST} . This is apparent contrary to the general understandings

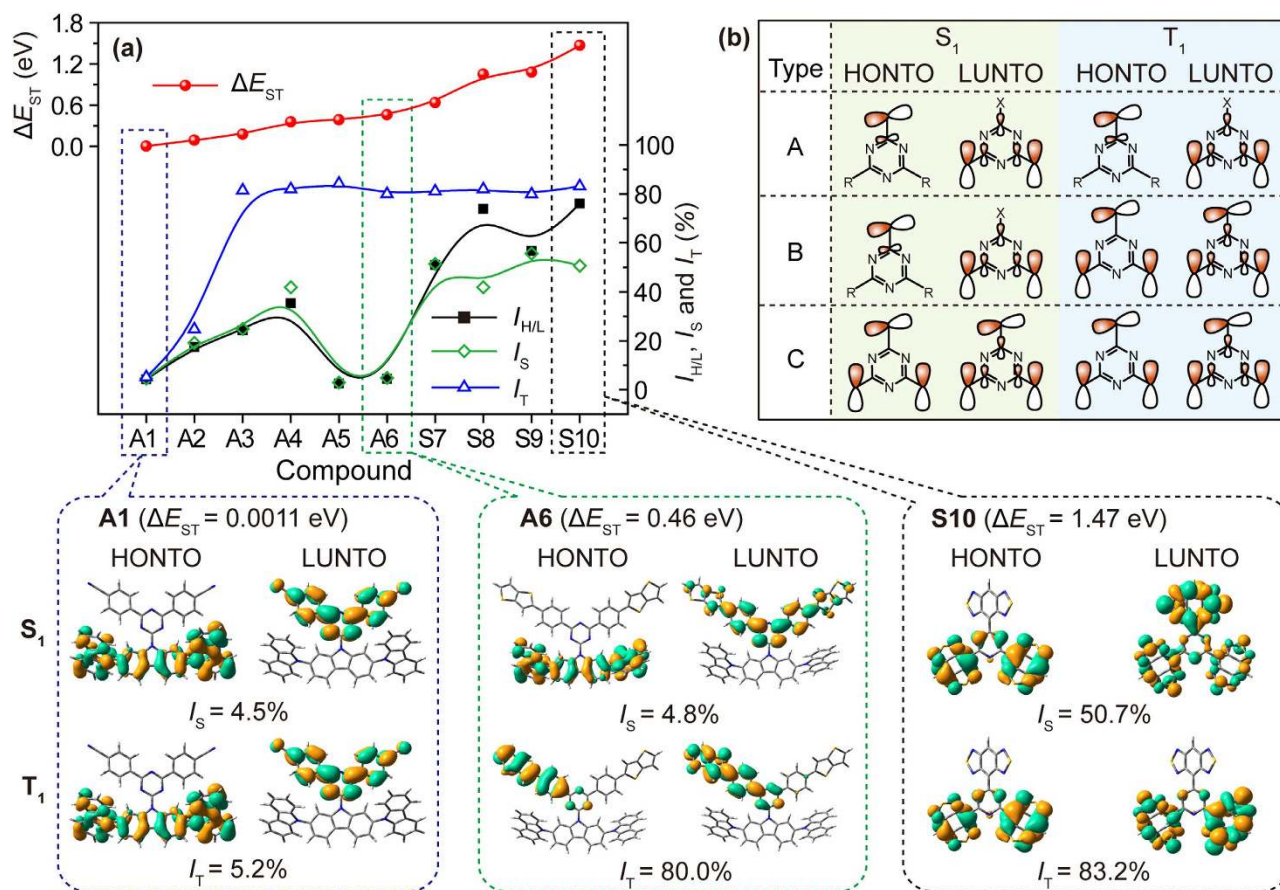


Figure 3. The influence of the frontier orbital overlap on ΔE_{ST} . (a) The relations between the calculated ΔE_{ST} , $I_{H/L}$, I_S and I_T of triazines. Insets: HONTO and LUNTO for S_1 and T_1 of **A1**, **A6**, and **S10** from left to right, respectively; (b) The types of triazines with different HONTO-LUNTO overlap patterns at S_1 and T_1 states.

expressed in equation (1–8), suggesting that there are also other undiscovered factors that influence ΔE_{ST} significantly.

The inconsistency between $I_{H/L}$ and ΔE_{ST} can be also observed in TADF molecules (compound **2** in Table S1) experimentally investigated by Adachi *et al.*¹¹ recently. Notably, this inconsistency may not be the calculations errors of B3LYP; other methods also well reproduced the mismatch between $I_{H/L}$ and ΔE_{ST} (Table S2). One main reason for this mismatch is possibly that it is not accurate to use only one transition mode of HOMO \rightarrow LUMO to describe the transition nature of S_1 or T_1 states. The TD-DFT calculations usually describe excited states in terms of various combinations of transitions between canonical molecular orbitals, and S_1 and T_1 are described by a set of transitions, e.g., HOMO \rightarrow LUMO, HOMO \rightarrow LUMO + 1, etc.³¹. Thus, a simple consideration of HOMO \rightarrow LUMO transition may overlook intrinsic photophysical essence, leading to false estimations of optoelectronic properties and ΔE_{ST} , especially when the content of HOMO \rightarrow LUMO transition is low or symmetrically forbidden. From Tables S1 and S3, the HOMO \rightarrow LUMO transition was absent in the compositions of T_1 of compounds **2**, **A5** and **A6**, leading to obviously mismatched $I_{H/L}$ and ΔE_{ST} .

The HONTO-LUNTO overlap extent. To consider a whole picture of electron transitions in excited states, natural transition orbital (NTO) analysis, obtained *via* the singular value decomposition of the 1-particle transition density matrix (T), was performed to offer a compact orbital representation for the electronic transition density matrix^{31,32}. All one electron properties associated with the transition can be interpreted in a transparent way as a sum over the occupied natural transition orbitals, each orbital being paired with a single unoccupied orbital, weighted with the appropriate eigenvalue, providing a convenient description of an excited state with fewer orbital pairs than the ones given on the basis of frontier molecular orbitals. The overlap extents between HONTO and LUNTO at S_1 (I_S) and T_1 (I_T) states, which take full considerations of electron transition components at the corresponding excited states, were also calculated using Multiwfn²⁴. From Fig. 3a, symmetric triazines generally have high I_S and I_T , but high I_T can be also observed in asymmetric molecules, leading to relatively large ΔE_{ST} of those compounds³³.

Typically, in compounds of **A5** and **A6** that were misunderstood by low $I_{H/L}$, their I_S are very low (<5%), but the I_T are around 80%, suggesting that there are severe overlaps at T_1 and the high I_T should be very likely the main reason for their relatively large ΔE_{ST} (~0.45 eV).

Take a close look at the HONTO and LUNTO distributions at S_1 and T_1 . When ΔE_{ST} is extremely low (0.0011 eV) as in **A1**, both HONTO and LUNTO are separated with low I_S and I_T (~5%); when ΔE_{ST} is relatively high (0.46 eV) as in **A6**, HONTO and LUNTO are separated at S_1 with low I_S (<5%) but they are overlapped at T_1 with high I_T (~80%); when HONTO and LUNTO are overlapped at both S_1 and T_1 with high I_S and I_T (~50% and 80% respectively) as in **S10**, very high ΔE_{ST} (1.47 eV) can be resulted. To this end, three types of molecules can be distinguished according to HONTO and LUNTO overlap pattern (Fig. 3b). In **Type A**, ultralow ΔE_{ST} is resulted from the separated HONTO and LUNTO at both S_1 and T_1 (small I_S and small I_T) states. In **Type B**, moderately low ΔE_{ST} can be observed with separated HONTO and LUNTO at S_1 state but overlapped HONTO and LUNTO at T_1 (small I_S but large I_T) state. **Type C** has large ΔE_{ST} due to overlapped HONTO and LUNTO at both S_1 and T_1 states (large I_S and large I_T). The newly revealed relation between ΔE_{ST} and overlap extents of I_S and I_T highlights the importance of full consideration of molecular orbital participations at related spin states, when studying the exciton transfer processes between these excited states. Notably, these finds are independent of TD-DFT computational functionals; as presented in Table 1, same relations can be also concluded from other computational methods.

The frontier orbital separation distance. The success in dividing molecules into **Types A, B, and C** according to I_S and I_T qualitatively cannot be achieved when analyzing their individual difference quantitatively. For example, **S7** has higher I_S and similar I_T in comparison with **S8**, but its ΔE_{ST} is quite lower than that of **S8**. The same inconsistency can be also found between **A4** and **A5**. From equation (3), ΔE_{ST} was determined not only by the molecular orbital overlap but also by their separation distance³⁴. Larger separation distance leads to lower ΔE_{ST} ³⁵. Hence, we need to further quantitatively investigate the effects of mean separation distances between HOMO and LUMO ($\langle r_{H/L} \rangle$), and between HONTO and LUNTO at S_1 ($\langle r_S \rangle$) and T_1 ($\langle r_T \rangle$).

From **A1** to **S10** whose ΔE_{ST} increases gradually, the expected gradually decreased $\langle r_{H/L} \rangle$ was broken obviously by **A5** and **A6**; **A5** has the largest $\langle r_{H/L} \rangle$ (Fig. 4a). This abnormal is in line with their unexpectedly low $I_{H/L}$ in Fig. 3a, indicating again the inaccuracy of $I_{H/L}$ and $\langle r_{H/L} \rangle$ in assessing ΔE_{ST} . Benefited from NTO analysis on the whole picture of the electron transitions for the excited states, the low $\langle r_T \rangle$ of **A5** and **A6** should be a main reason for their high ΔE_{ST} , although their $\langle r_S \rangle$ are also quite high. Notably, symmetric triazines generally have lower $\langle r_{H/L} \rangle$, $\langle r_S \rangle$, and $\langle r_T \rangle$ than asymmetric triazines, resulting in the high ΔE_{ST} according to equation (3).

To elucidate quantitative relations between ΔE_{ST} and factors of $I_{H/L}$ and $\langle r_{H/L} \rangle$, we simplified equation (3) to get equation (9) (see Supplementary Information).

$$\Delta E_{ST} = 28.8 \frac{I_{H/L}^2}{\langle r_{H/L} \rangle} \quad (9)$$

where ΔE_{ST} is in eV and $\langle r_{H/L} \rangle$ is in Å. From the 35 compounds except for **A5** and **A6**, the average $\Delta E_{ST}/(I_{H/L}^2/\langle r_{H/L} \rangle)$ is 25.7 (Fig. S6)³⁶, which is very close to the 28.8 in equation (9). The very high values observed in **A5** and **A6** (Fig. 4b) suggest again the unfitness of the normal HOMO-LUMO transition analysis, since there are very low HOMO \rightarrow LUMO transition components for their T_1 states. Therefore, it is necessarily to address not only the conventional HOMO \rightarrow LUMO transition but also the other frontier orbital transition components.

With the aid of NTO analysis to contain all the possible transitions, new parameters of I_S , I_T , $\langle r_S \rangle$, and $\langle r_T \rangle$ were obtained and found to be useful in investigating the influence factors of ΔE_{ST} . The quantitative relations were supposed to be a linear combination of S_1 and T_1 components in equation (10):

$$\Delta E_{ST} = C_S \frac{I_S^2}{\langle r_S \rangle} + C_T \frac{I_T^2}{\langle r_T \rangle} \quad (10)$$

where C_S and C_T are combination constants of S_1 and T_1 states, respectively. From all the compounds studied (**A1**~**S37**) including **A5** and **A6**, the nonlinear least square fitted C_S and C_T are found to be 0.23 and 0.39 respectively with R-square of 0.9685. If C_S is set to be equal to C_T , they were changed to 0.385 with R-square of 0.9912. The higher C_T than C_S in the first fit with slight decrease in the second fit, suggests that the T_1 component plays a dominate role in determining ΔE_{ST} . For all the 37 studied compounds, $\Delta E_{ST}/(I_S^2/\langle r_S \rangle + I_T^2/\langle r_T \rangle)$ varies in a relatively narrow range from 0.15 to 11.16 (Fig. 4b and S6), indicating that the simplified equation (10) presents a good correlation between ΔE_{ST} and parameters of I_S , I_T , $\langle r_S \rangle$, and $\langle r_T \rangle$ derived from NTO analysis. Thus, it is advisable to consider the whole picture of frontier orbital transitions (HONTO and LUNTO) at both S_1 and T_1 states to accurately understand ΔE_{ST} tuning.

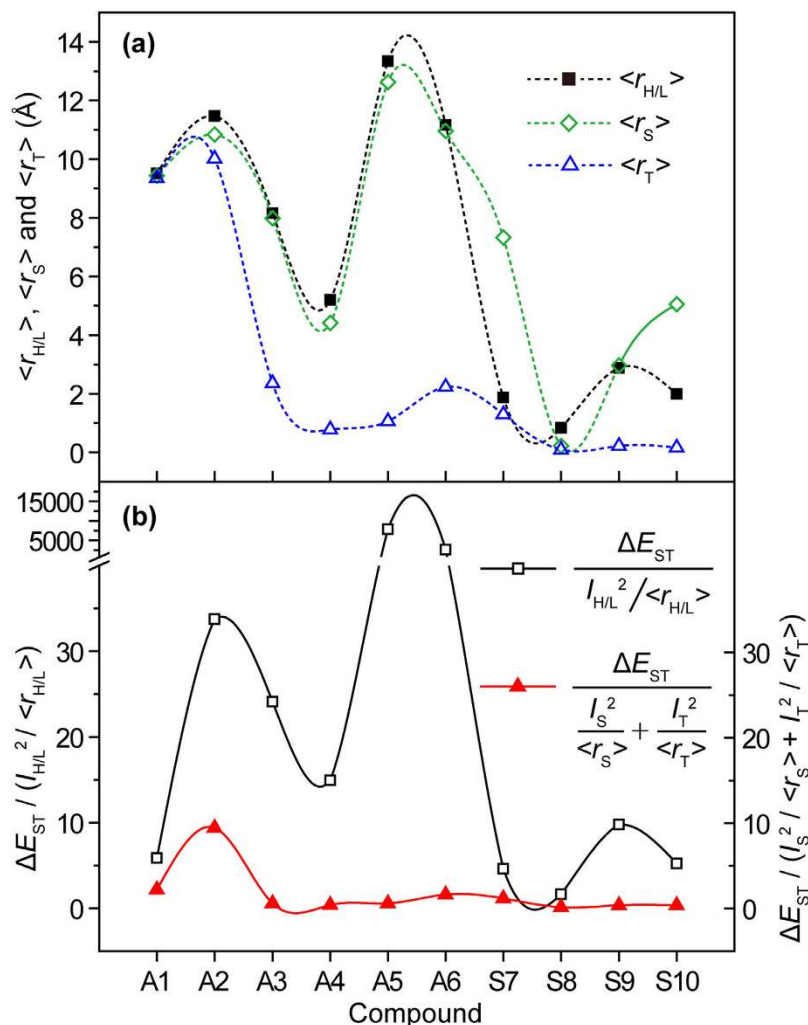


Figure 4. The influence of the frontier orbital separation distance on ΔE_{ST} . (a) The $\langle r_{H/L} \rangle$, $\langle r_S \rangle$ and $\langle r_T \rangle$. (b) The values of $\Delta E_{ST}/(I_{H/L}^2/\langle r_{H/L} \rangle)$ and $\Delta E_{ST}/(I_S^2/\langle r_S \rangle + I_T^2/\langle r_T \rangle)$.

Design of ideal TADF molecules with ultralow ΔE_{ST} . In light of the sophisticated tuning of ΔE_{ST} via symmetric control on I_S and I_T and distance control on $\langle r_S \rangle$ and $\langle r_T \rangle$, we first use the above developed molecular design strategy to construct high-performance TADF molecules with ultralow ΔE_{ST} ; the development of novel TADF molecules is one of the hottest topics in current research of organic electronics⁸. To test the validity of the above studies on the relations between ΔE_{ST} and these new parameters of $I_{H/L}$, I_S , I_T , $\langle r_{H/L} \rangle$, $\langle r_S \rangle$ and $\langle r_T \rangle$, four efficient TADF molecules recently reported by Adachi and co-workers¹¹ was investigated. Indeed, the smaller $I_{H/L}$ cannot lead to lower ΔE_{ST} ; the larger ΔE_{ST} can be explained by the larger I_T of these molecules (Table S1); the higher I_S with higher frontier orbital overlap at S_1 state may lead to higher luminescent efficiency of the D-A molecules when the low I_T can still maintain a small ΔE_{ST} . Still, these finds are independent of calculation methods (Table S2). Our approach gave a good prediction on the reported experimental results, indicating the high reliability of these new parameters for ΔE_{ST} describing.

Based on triazine architecture, we adopt an asymmetric molecular structure to minimize ΔE_{ST} by fine-tuning the substitution positions and varied types of donor and acceptor substituents³⁷. Started from the asymmetric triazine molecule of **A3**, which is an efficient host material for phosphorescent OLED with experimental ΔE_{ST} of 0.34 eV²⁷, we enhanced the electron donating ability of the carbazolyl substituent by introducing additional donors of carbazole at 2,7- or 3,6- position; on the other hand, we enhanced the electron accepting ability of the two phenyl substituents by attaching the strong acceptor of cyano group (CN) at the *para* (*p*), *meta* (*m*), or *ortho* (*o*) positions (Fig. 5a). According to the TD-DFT calculations, this strategy is succeed in producing ultralow (almost zero) ΔE_{ST} especially in **A1**, **A13**, and **A14**, when the additional donors are connected through 2,7-positions of the carbazolyl substituent and the CN is introduced either at *p*, *m*, or *o* position. The 3,6- connection results in slight HOMO distribution on triazine core, which will overlap with LUMO distribution, leading to slightly higher ΔE_{ST} of **A11** (Table S4 and Fig. S5a). Besides carbazolyl substituents, other electron donating groups such as

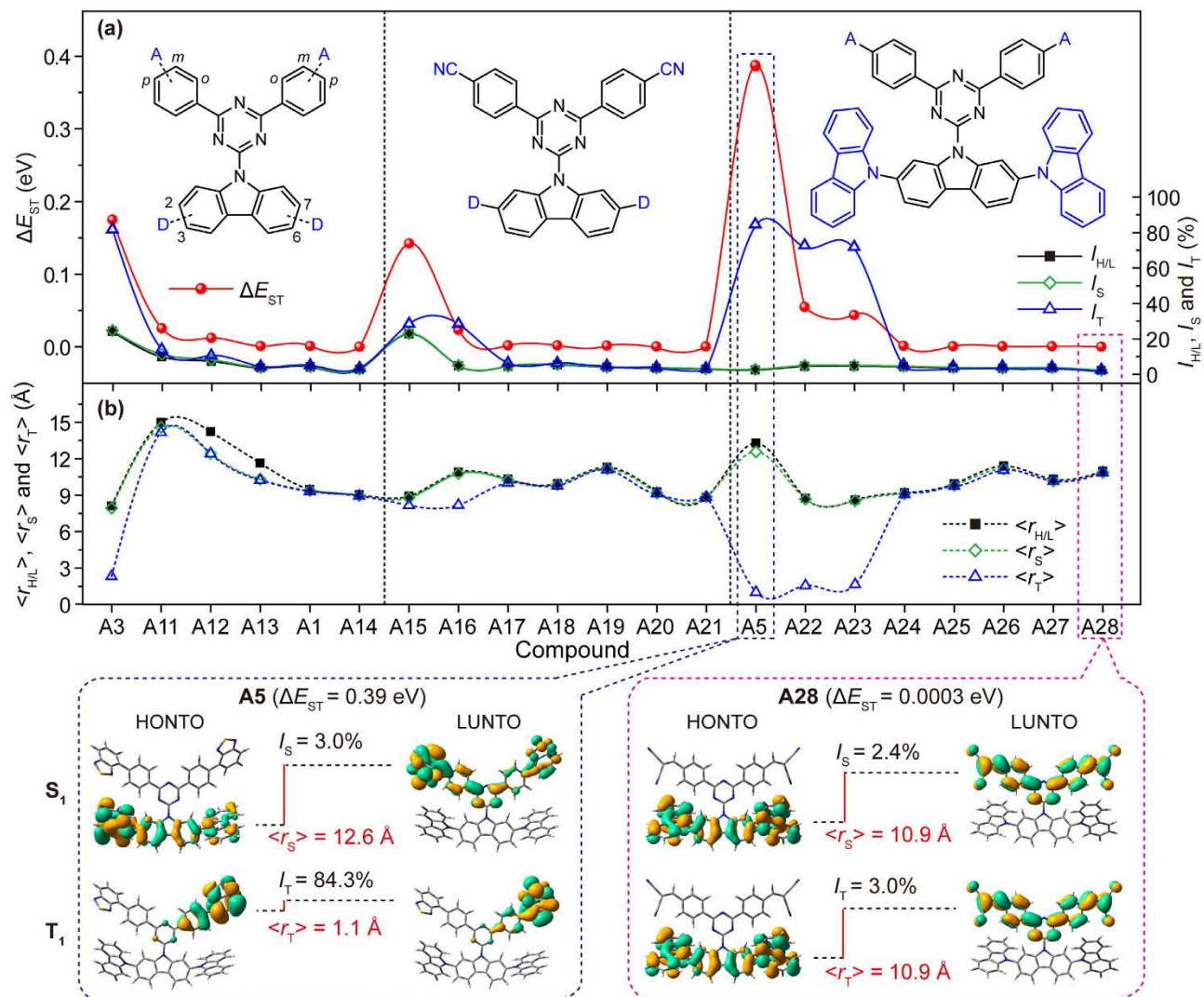


Figure 5. The ΔE_{ST} of the designed asymmetric triazines TADF molecules. (a) The overlap extents of $I_{H/L}$, I_S and I_T and (b) the average frontier orbital separation distances of $\langle r_{H/L} \rangle$, $\langle r_S \rangle$ and $\langle r_T \rangle$. Insets: HONTO and LUNTO for S_1 and T_1 of A5 (left) and A28 (right).

alkyl, phenyl, diamine, alkoxy, etc. as in A16~A21, are also effective in reducing ΔE_{ST} (Fig. S5b). But, without the additional donors to increase the HOMO, ΔE_{ST} will be apparently increased as found in A15. Also, without the additional acceptors on the phenyl substituents to reduce the LUMO, ΔE_{ST} will be large as in A22. Still, other kinds of accepting groups of trifluoromethyl, diphenylphosphoryl, nitril, diphenylboronyl, and 2-methylenemalononitrile in A24~A28, work well too, producing ultralow ΔE_{ST} (low to 0.0003 eV in A28) (Fig. S5c). However, fluoro and benzothiazolyl substitution cannot lead to low ΔE_{ST} due to their failure in avoiding overlap at both S_1 and T_1 ; the large I_T and small $\langle r_T \rangle$ of A5 and A23 clearly indicates the large overlap at T_1 states (Fig. 5a,b). Compared to the experimentally investigated TADF molecule of A2, which has exhibited an external quantum efficiency (EQE) of $14\% \pm 1\%$ with the experimental ΔE_{ST} of 0.02 eV and calculated one of 0.09 eV based on B3LYP/6-31G(d) (Table 1)²⁸, these newly designed TADF molecules are expected to have improved device performance, considering their well separated S_1 and T_1 with low I_S and I_T and long $\langle r_S \rangle$ and $\langle r_T \rangle$ simultaneously.

Design of TTA and SF molecules with large ΔE_{ST} . Contrary to the asymmetric triazine-based TADF molecules showing very low ΔE_{ST} , symmetric triazines can lead to large ΔE_{ST} which is required for TTA and SF molecules. According to equation (9) and (10), large ΔE_{ST} needs large $I_{H/L}$, I_S , and I_T as well as short $\langle r_{H/L} \rangle$, $\langle r_S \rangle$, and $\langle r_T \rangle$. In other words, large transition orbital overlap with localized excitation will result in large ΔE_{ST} ³⁴. Here, two approaches were adopted to design symmetric triazine-based TTA and SF molecules. The first one is to use electron-withdrawing substituents to make the S_1 and T_1 locally excited. The other one is by introducing polycyclic aromatic fragments, which have

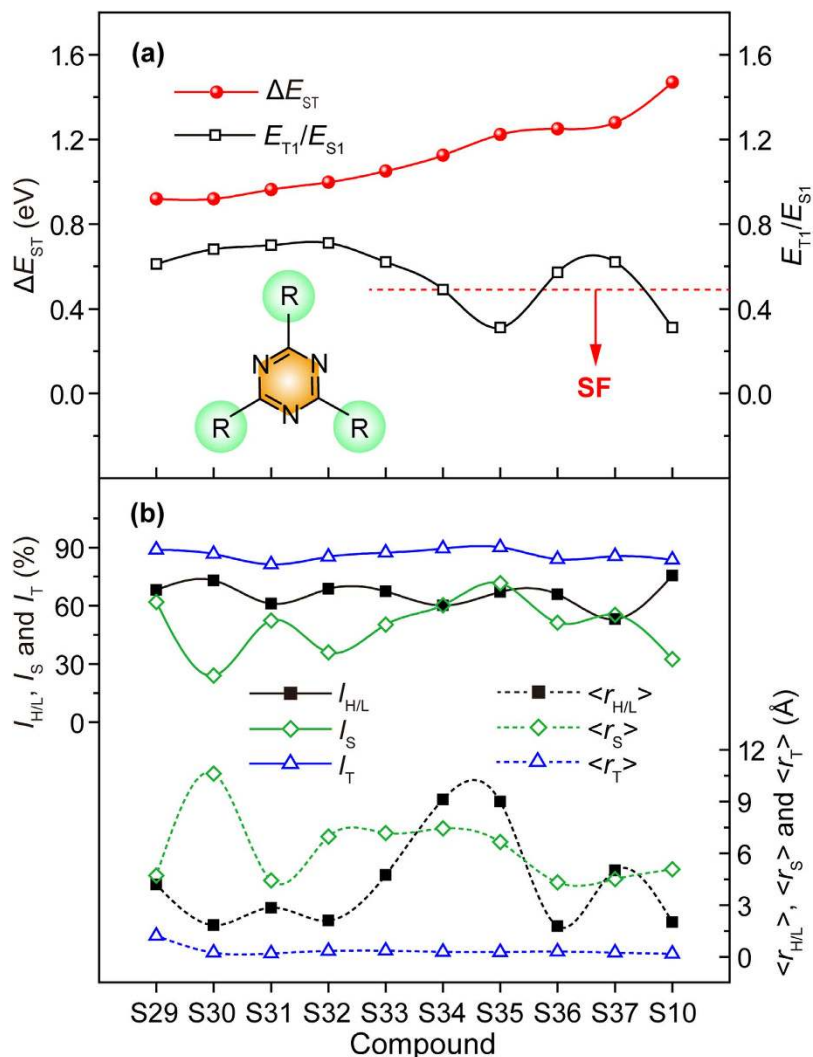


Figure 6. The designed symmetric triazines for TTA and SF. (a) ΔE_{ST} and E_{T1}/E_{S1} ; (b) $I_{H/L}$, I_S , I_T , $\langle r_{H/L} \rangle$, $\langle r_S \rangle$ and $\langle r_T \rangle$.

been widely used in many TTA and SF molecules due to their large conjugation beneficial for electron localization at excited states.

In Fig. 6a, the molecules are arranged in an increasing order of ΔE_{ST} from 0.92 to 1.47 eV. When E_{T1}/E_{S1} is close but higher than 0.5, TTA process is supposed potentially to be applicable; when E_{T1}/E_{S1} is lower than 0.5, SF process is possible^{18,19}. According to these criterions, **S10**, **S34**, and **S35** are SF molecules, while **S29** ~ **S33**, **S36** and **S37** are TTA molecules. From Fig. S7, the electron acceptor of triazine core participates the formation of LUMO to a large content for all the symmetric compounds, while it shows only apparent effects on HOMOs of **S36** and **S37** whose substituents are acceptors, because HOMO is dominated by the donor unit in D-A molecules. Delocalized HONTO and LUNTO at both S_1 and T_1 of **S36** was also observed, which is in contradictory to the D-A molecule of **S35** (Fig. S8a and b). The more localized and overlapped HONTO and LUNTO of **S35** makes it a good SF molecule with lower E_{T1} and E_{T1}/E_{S1} . Notably, the increase of ΔE_{ST} will not certainly leads to SF molecules; the T_1 energy of **S36** and **S37** are comparably too high (Table S5), resulting in $E_{T1}/E_{S1} > 0.5$, although their ΔE_{ST} are among the largest ones. The high-lying T_1 may have close relations with the triazine core³⁸. The large participation of the triazine core at T_1 of **S36** was further confirmed by its delocalized spin density distribution (Fig. S8c). Since the triazine core has high T_1 , its large participation may enable the compound to inherit the high T_1 of triazine, resulting in high E_{T1}/E_{S1} of **S36** and **S37**.

From Fig. 6b, significantly higher $I_{H/L}$ and shorter $\langle r_{H/L} \rangle$ of the symmetric triazines in comparison with that of asymmetric triazines were observed, demonstrating the success in modifying the molecular orbital overlap and separation distance *via* symmetry control in designing molecules with large ΔE_{ST} for TTA or SF processes. As further revealed by I_S and I_T , heavier overlap seems to happen at T_1 with much shorter $\langle r_T \rangle$ than $\langle r_S \rangle$, highlighting the dominative role of T_1 in the enlargement of ΔE_{ST} . For the construction of triazine-based TTA and TADF molecules, they can be facily designed by symmetrically

introducing TTA molecules of perylene, pyrene, and anthracene or SF molecules of naphthacene and pentacene correspondingly. Typically, the S_1 energy of **S10** with the largest ΔE_{ST} of 1.47 eV is more than twice higher than its T_1 energy, affording **S10** to be a good candidate for SF process¹⁸.

Discussion

We have succeed in manipulating excited state electronic structures for accommodation of various organic excitons *via* symmetry control of ΔE_{ST} in a wide range from ultralow (0.0003 eV) for TADF and extra-large (1.47 eV) for SF all in a triazine-based molecular architecture based on a combined quantum chemistry modeling and experimental exploring. The HOMO-LUMO overlap ($I_{H/L}$) and separation distance ($\langle r_{H/L} \rangle$) were quantified successfully. It was found that asymmetry triazines possess separated HOMO-LUMO with low $I_{H/L}$ and long $\langle r_{H/L} \rangle$, leading to low ΔE_{ST} ; while symmetry triazines contain highly overlapped HOMO-LUMO with high $I_{H/L}$ and short $\langle r_{H/L} \rangle$, resulting in large ΔE_{ST} . However, it is difficult for $I_{H/L}$ and $\langle r_{H/L} \rangle$ to well describe ΔE_{ST} . Consequently, we further developed a set of new parameters of I_S , I_T , $\langle r_S \rangle$, and $\langle r_T \rangle$ benefitted from NTO analysis to consider whole pictures of the electron transitions at both S_1 and T_1 states. According to these firstly proposed parameters, three types of molecules can be classified. **Type A** has ultralow ΔE_{ST} due to both separated S_1 and T_1 with low I_S (long $\langle r_S \rangle$) and I_T (long $\langle r_T \rangle$); **Type B** has small ΔE_{ST} due to separated S_1 but overlapped T_1 with low I_S (long $\langle r_S \rangle$) and high I_T (short $\langle r_T \rangle$); **Type C** shows large ΔE_{ST} due to overlapped S_1 and T_1 with high I_S (short $\langle r_S \rangle$) and I_T (short $\langle r_T \rangle$). A quantitative relation between ΔE_{ST} and I_S , I_T , $\langle r_S \rangle$, and $\langle r_T \rangle$ was established and the T_1 component was found to play a dominate role in determining ΔE_{ST} . These findings are important in providing quantitative approaches for fundamental understandings on the intrinsic factors influencing ΔE_{ST} tuning, representing a major step towards technological advances in expanding the scope of excited state manipulation.

Methods

The molecular geometries in the ground state (S_0) were optimized *via* spin-restricted DFT calculations at the B3LYP/6-31G(d) level of theory using Gaussian 09 package³⁹. The spin-unrestricted formalism was used in geometry optimization of the lowest triplet excited state (T_1). Vibrational frequency calculations were subsequently carried out to confirm that all the optimized structures are corresponding to the minima on the potential energy surfaces. The excited singlet (S_n) and triplet (T_n) states were investigated by the time-dependent DFT (TD-DFT) formalism with the same functional and basis set of B3LYP/6-31G(d) on the optimized ground-state geometries⁴⁰. TD-DFT calculations based on the standard B3LYP functional offer a reasonable description for singlet and triplet states of medium-sized molecules, which has been widely used in the theoretical studies of TADF, TTA and SF molecules^{11,41}. To obtain a precise picture of the excited states, we further performed natural transition orbitals (NTOs) analysis, which can offer a compact orbital representation for the electronic transition density matrix³⁶.

To get a solid support of the computational study, the experimental measurements of the synthesized triazines were analyzed and compared. The detailed synthesis, structure characterizations, and photo-physical property measurements of these triazines can be found in Supplementary Information.

References

1. Figueira-Duarte, T. M. & Muellen, K. Pyrene-based materials for organic electronics. *Chem. Rev.* **111**, 7260–7314 (2011).
2. Wang, C., Dong, H., Hu, W., Liu, Y. & Zhu, D. Semiconducting π -conjugated systems in field-effect transistors: a material odyssey of organic electronics. *Chem. Rev.* **112**, 2208–2267 (2012).
3. Tang, C. W. & VanSlyke, S. A. Organic electroluminescent diodes. *Appl. Phys. Lett.* **51**, 913–915 (1987).
4. Baldo, M. A. *et al.* Highly efficient phosphorescent emission from organic electroluminescent devices. *Nature* **395**, 151–154 (1998).
5. Birks, J. B. *Photophysics of aromatic molecules* Wiley-Interscience, New York, 1970.
6. Pope, M. & Swenberg, C. E. *Electronic processes in organic crystals and polymers* [2nd (ed.)] Oxford University Press, Oxford, UK, 1999.
7. Uoyama, H., Goushi, K., Shizu, K., Nomura, H. & Adachi, C. Highly efficient organic light-emitting diodes from delayed fluorescence. *Nature* **492**, 234–238 (2012).
8. Tao, Y. *et al.* Thermally activated delayed fluorescence materials towards the breakthrough of organoelectronics. *Adv. Mater.* **26**, 7931–7958 (2014).
9. Chou, P. Y. *et al.* Efficient delayed fluorescence via triplet-triplet annihilation for deep-blue electroluminescence. *Chem. Commun.* **50**, 6869–6871 (2014).
10. Congreve, D. N. *et al.* External quantum efficiency above 100% in a singlet-exciton-fission-based organic photovoltaic cell. *Science* **340**, 334–337 (2013).
11. Hirata, S. *et al.* Highly efficient blue electroluminescence based on thermally activated delayed fluorescence. *Nat. Mater.* **14**, 330–336 (2015).
12. Sun, J. W. *et al.* A fluorescent organic light-emitting diode with 30% external quantum efficiency. *Adv. Mater.* **26**, 5684–5688 (2014).
13. Xu, H. *et al.* Recent progress in metal-organic complexes for optoelectronic applications. *Chem. Soc. Rev.* **43**, 3259–3302 (2014).
14. Monkman, A. P. Singlet generation from triplet excitons in fluorescent organic light-emitting diodes. *ISRN Mater. Sci.* **2013**, 1–19 (2013).
15. Leitl, M. J., Krylova, V. A., Djurovich, P. I., Thompson, M. E. & Yersin, H. Phosphorescence versus thermally activated delayed fluorescence. Controlling singlet-triplet splitting in brightly emitting and sublimable Cu(I) compounds. *J. Am. Chem. Soc.* **45**, 16032–16038 (2014).
16. Parker, C. A. & Hatchard, C. G. Triplet-singlet emission in fluid solutions. Phosphorescence of eosin. *Trans. Faraday Soc.* **57**, 1894–1904 (1961).

17. Zhou, J. *et al.* Charge-transfer-featured materials-promising hosts for fabrication of efficient OLEDs through triplet harvesting via triplet fusion. *Chem. Commun.* **50**, 7586–7589 (2014).
18. Smith, M. B. & Michl, J. Singlet fission. *Chem. Rev.* **110**, 6891–6936 (2010).
19. Simon, Y. C. & Weder, C. Low-power photon upconversion through triplet-triplet annihilation in polymers. *J. Mater. Chem.* **22**, 20817–20830 (2012).
20. Lee, S. Y., Yasuda, T., Nomura, H. & Adachi, C. High-efficiency organic light-emitting diodes utilizing thermally activated delayed fluorescence from triazine-based donor-acceptor hybrid molecules. *Appl. Phys. Lett.* **101**, 93306 (2012).
21. Monahan, N. & Zhu, X. Y. Charge transfer-mediated singlet fission. *Annu. Rev. Phys. Chem.* **66**, 601–618 (2015).
22. Busby, E. *et al.* A design strategy for intramolecular singlet fission mediated by charge-transfer states in donor-acceptor organic materials. *Nat. Mater.* **14**, 426–433 (2015).
23. Endo, A. *et al.* Thermally activated delayed fluorescence from sn^{4+} -porphyrin complexes and their application to organic light emitting diodes—a novel mechanism for electroluminescence. *Adv. Mater.* **21**, 4802–4806 (2009).
24. Lu, T. & Chen, F. Multiwfn: a multifunctional wavefunction analyzer. *J. Comput. Chem.* **33**, 580–592 (2012).
25. Lu, T. Multiwfn: a multifunctional wavefunction analyzer version 3.3.3, 2013.
26. An, Z. *et al.* Modulation of singlet and triplet excited states through σ spacers in ternary 1,3,5-triazines. *RSC Adv.* **3**, 13782–13788 (2013).
27. An, Z. *et al.* Conjugated asymmetric donor-substituted 1,3,5-triazines: new host materials for blue phosphorescent organic light-emitting diodes. *Chem. Eur. J.* **17**, 10871–10878 (2011).
28. Sato, K. *et al.* Organic luminescent molecule with energetically equivalent singlet and triplet excited states for organic light-emitting diodes. *Phys. Rev. Lett.* **110**, 247401 (2013).
29. Yin, J., Zhang, S., Chen, R., Ling, Q. & Huang, W. Carbazole endcapped heterofluorenes as host materials: theoretical study of their structural, electronic, and optical properties. *Phys. Chem. Chem. Phys.* **12**, 15448–15458 (2010).
30. Zhou, H., Yang, L., Price, S. C., Knight, K. J. & You, W. Enhanced photovoltaic performance of low-bandgap polymers with deep LUMO levels. *Angew. Chem. Int. Edit.* **49**, 7992–7995 (2010).
31. Kim, D., Coropceanu, V. & Brédas, J. Design of efficient ambipolar host materials for organic blue electrophosphorescence: theoretical characterization of hosts based on carbazole derivatives. *J. Am. Chem. Soc.* **133**, 17895–17900 (2011).
32. Salman, S., Kim, D., Coropceanu, V. & Brédas, J. Theoretical investigation of triscarbazole derivatives as host materials for blue electrophosphorescence: effects of topology. *Chem. Mater.* **23**, 5223–5230 (2011).
33. Moral, M., Muccioli, L., Son, W. J., Olivier, Y. & Sancho-García, J. C. Theoretical rationalization of the singlet-triplet gap in OLEDs materials: impact of charge-transfer character. *J. Chem. Theory Comput.* **11**, 168–177 (2015).
34. Köhler, A. & Beljonne, D. The singlet-triplet exchange energy in conjugated polymers. *Adv. Funct. Mater.* **14**, 11–18 (2004).
35. Zhang, Q. *et al.* Anthraquinone-based intramolecular-charge-transfer compounds: computational molecular design, thermally activated delayed fluorescence, and highly-efficient red electroluminescence. *J. Am. Chem. Soc.* **52**, 18070–18081 (2014).
36. Martin, R. L. Natural transition orbitals. *J. Chem. Phys.* **118**, 4775–4777 (2003).
37. Valchanov, G., Ivanova, A., Tadjer, A., Chercka, D. & Baumgarten, M. Tuning the optical absorption of potential blue emitters. *Org. Electron.* **14**, 2727–2736 (2013).
38. An, Z. *et al.* Exceptional blueshifted and enhanced aggregation-induced emission of conjugated asymmetric triazines and their applications in superamplified detection of explosives. *Chem. Eur. J.* **18**, 15655–15661 (2012).
39. Frisch, M. J. *et al.* Gaussian 09 Gaussian, Inc.: Wallingford, CT, 2009.
40. Yin, J., Chen, R., Zhang, S., Ling, Q. & Huang, W. Theoretical studies of the structural, electronic, and optical properties of phosphafuorenes. *J. Phys. Chem. A* **114**, 3655–3667 (2010).
41. Milián-Medina, B. & Gierschner, J. Computational design of low singlet-triplet gap all-organic molecules for OLED application. *Org. Electron.* **13**, 985–991 (2012).

Acknowledgements

This study was supported in part by the National Natural Science Foundation of China (21274065, 21304049, 21001065, 61136003, and 51173081), The Ministry of Education of China (No. IRT1148), a project funded by the priority academic program development of Jiangsu higher education institutions (PAPD, YX03001), the Qing Lan project of Jiangsu province, and the National Basic Research Program of China (973 Program) (2012CB933301, 2012CB723402, and 2014CB648300).

Author Contributions

T.C. and R.C. wrote the manuscript. T.C. carried out the quantum chemistry calculations. L.Z., J.Y. and Z.A. performed the experiments. L.Z., Y.T., H.L., X.X. and W.H. helped to prepare the figures and proofread the manuscript. All authors reviewed the manuscript.

Additional Information

Supplementary information accompanies this paper at <http://www.nature.com/srep>

Competing financial interests: The authors declare no competing financial interests.

How to cite this article: Chen, T. *et al.* Understanding the Control of Singlet-Triplet Splitting for Organic Exciton Manipulating: A Combined Theoretical and Experimental Approach. *Sci. Rep.* **5**, 10923; doi: 10.1038/srep10923 (2015).



This work is licensed under a Creative Commons Attribution 4.0 International License. The images or other third party material in this article are included in the article's Creative Commons license, unless indicated otherwise in the credit line; if the material is not included under the Creative Commons license, users will need to obtain permission from the license holder to reproduce the material. To view a copy of this license, visit <http://creativecommons.org/licenses/by/4.0/>